Electromagnetic Control of Separation at Hydrofoils

Gerd MUTSCHKE[1], Tom WEIER[1], Thomas ALBRECHT[2], Gunter GERBETH[1] and Roger GRUNDMANN[2].

[1] *Forschungszentrum Dresden-Rossendorf, MHD Dept., PO Box 510119, 01314 Dresden, Germany*
[2] *Dresden University of Technology, Inst. Aero. Eng., 01062 Dresden, Germany*

Abstract. Lorentz forces originating from surface-mounted actuators of permanent magnets and electrodes in weakly conducting fluids like seawater provide a convenient tool for separation control at hydrofoils. A well-known actuator design of alternating stripes of permanent magnets and externally fed electrodes is considered which creates a mainly streamwise Lorentz force that is exponentially decaying in wall-normal direction. Separation control by steady forcing at the suction side and by oscillatory forcing near the leading edge of a symmetric foil is investigated numerically, mostly in the post-stall regime. The results are based on direct numerical simulations in the laminar flow regime in order to reveal basic control phenomena as well as on simulations using turbulence modelling at higher Reynolds numbers which are closer to possible naval application. By applying a strong enough steady control, separation can always be completely suppressed. The scaling behaviour of the maximum lift gain ΔC_L^{max} in the turbulent regime nicely agrees with experimental results. – Oscillatory forcing always has to compete with the natural shedding process, lock-in behavior may occur. Lift-optimum control for strong amplitudes is found in a frequency band around the natural shedding frequency. In terms of the momentum coefficient describing the control effort, appropriate excitation frequencies in relation to the natural vortex shedding frequency allow for a more effective lift control than steady forcing for small lift gains; for large lift enhancement the energetic effort seems to approach the level of steady control.

Key words: electromagnetic flow control, separation control, wings, numerical simulation, incompressible flow.

1. Introduction

Separation control is an important issue in many industrial, aviation and marine applications, and a large variety of different control methods does exist [1]. Apart from steady control schemes, active control allows for more distinct benefits in certain flow configurations, as, e.g., proper time-periodic blowing and suction is known to enhance the lift of airfoils quite effectively as compared to steady blowing. Greenblatt and Wygnanski [2] attribute this effect to the periodic excitation of the separating shear-layer, thereby using far-field momentum to advantageously reorganize the vortex shedding process at the suction side. Optimum control frequencies with respect to lift enhancement found there are typically of $O(1)$ based on chord length and free stream velocity. Wu et. al [3] have performed two-dimensional RANS simulations of the turbulent flow over an airfoil at post-stall angles of attack when periodic blowing-suction near the leading edge is applied. Interestingly, in certain control parameter ranges, the still separated flow became periodic or quasi-periodic, associated with significant lift enhancement. The physical mechanisms responsible for this control are explained to be the non-linear mode competition of the two basic constituents of the flow, the leading-edge shear layer and the vortex shedding from the trailing edge.

The present paper is concerned with separation control by applying Lorentz forces into the near-wall region of an hydrofoil by surface setups of electrodes and magnets. We have in mind saltwater or electrolyte flows of weak electric conductivity ($\sigma \sim O(10)S/m$) where induction effects can be neglected and, besides externally applied magnetic fields, electric currents are fed to the fluid in order to generate Lorentz forces large enough for achieving control. Due to the momentum modification of the near-wall flow, a similarity to control by suction or blowing does exist. However, an obvious advantage of the Lorentz force approach is that its amplitude is easily adjustable in time by applying alternating currents up to high frequencies. First efforts in applying Lorentz forces to weakly-conducting fluids were undertaken more than 40 years ago [4, 5]. Meanwhile, control of transition in a flat-plate boundary layer [6], control of the turbulent boundary layer with respect to drag reduction [7–12] and control of the flow around a circular cylinder [13, 14] have been discussed extensively. Hoarau et al. [19] have investigated the 3-D transition around a NACA-0012 airfoil, and recently, first results on the separation control of flow around hydrofoils were published [15–17].

Although most potential control problems experience turbulent flow conditions, there is also particular interest in the transitional and low-Reynolds-number range for, e.g. RPV's and UAV's in aviation or for, e.g., active hydrofoils in naval applications. In this paper, we first present DNS results which are limited to relatively low chord Reynolds numbers but aimed to understand basic control effects. Second, results of turbulent simulations are presented and compared with experimental results. Both, steady and oscillatory control, are investigated in a first step of 2-D simulations as the surface tangential forcing weakens possible 3-D side effects in both laminar and turbulent flows. The basic mechanisms of time-periodic control were recently proven to work in the transitional range as control was achieved by conventional blowing/suction [18] as well as by applying Lorentz forces in experiments [15, 16]. In rotary or oscillatory control of the cylinder flow, in the literature several authors have reported on a lock-in behaviour between excitation frequency and vortex shedding frequency [21–24], and appropriate control techniques can lead to, e.g., considerably reduced drag values [25, 26]. Therefore, also for the oscillatory control at an hydrofoil considered here, a large control receptivity at excitation frequencies close to the main shedding frequency of the uncontrolled flow should be expected.

2. Problem definition

2.1. Hydrofoil and Actuator

A particular profile named PTL-4 was chosen to allow later for comparison with experimental results. The characteristic polynom of the foil is

$$p(x) = d(a_1\sqrt{x} + a_2x + a_3x^2 + a_4x^3 + a_5x^4) \quad (1)$$

with the coefficients $d = 0.1676154$, $a_1 = 1.26854$, $a_2 = -0.292071$, $a_3 = -1.34964$, $a_4 = 0.478002$, $a_5 = -0.104831$. Hereby, $0 \le x \le 1$ denotes the streamwise coordinate scaled with the chordlength c. As can be seen from the left side of Fig. 1, the

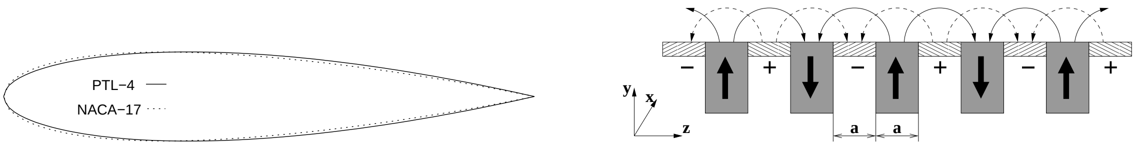

Figure 1. Left: Comparison of the PTL-4 hydrofoil with the shape of a NACA-17 profile. Right: Sketch (cross-cut) of the actuator for generating a streamwise (x) Lorentz force

shape is rather close to that of a standard NACA-0017 profile.
Lorentz forces $\mathbf{f}_L$ result from the cross product of current density $\mathbf{j}$ and magnetic induction $\mathbf{B}$, whereby the current density is given by Ohm's law in moving media $\mathbf{j} = \sigma(\mathbf{E} + \mathbf{u} \times \mathbf{B})$. Neglecting induction, in the following we assume that only the externally applied current density $\mathbf{j}_0 = \sigma \mathbf{E}_0$ and the applied magnetic field $\mathbf{B}_0$ contribute to the Lorentz force. A sketch of the actuator (cross-cut) is shown in the right side of Fig. 1. It consists of an alternating arrangement of stripes of electrodes of varying polarity and permanent magnets of varying magnetization direction (black arrows). The width of both electrodes and permanent magnets is assumed to be equal to a. Surface flush mounted, due to the crossing electric (dashed) and magnetic (solid) field lines, it creates a mainly streamwise (x) Lorentz volume force in the fluid which, when averaging over the spanwise direction z, reads

$$\mathbf{f}_L = \frac{\pi}{8} j_0 M_0 e^{-\frac{\pi}{a} y} \mathbf{e}_x \, . \tag{2}$$

Hereby, M_0 denotes the magnetization of the magnet. The spacing parameter a determines the "penetration depth" of the Lorentz force; larger values of a lead to Lorentz forces acting deeper inside the fluid. For more details we refer to [6]. Figure

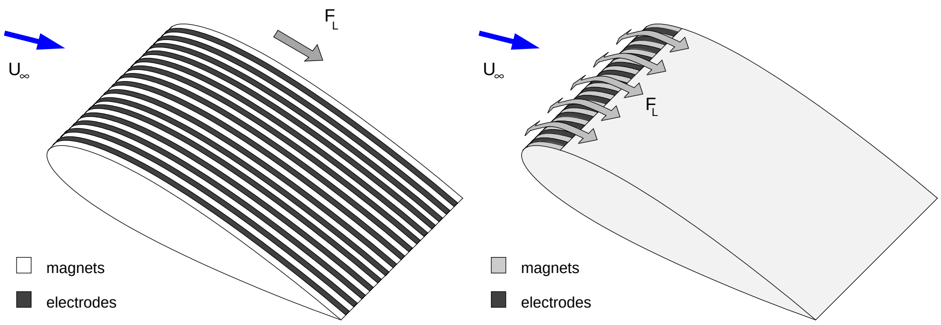

Figure 2. Foil with actuator for steady (left) and time-periodic (right) separation control

2 illustrates the actuator at the suction side of the hydrofoil for steady (left) and time-periodic (right) separation control.

2.2. Equations and Parameter

Based on chord length c of the hydrofoil and freestream velocity U_0, the 2-D Navier-Stokes equation for an incompressible fluid ($\nabla \cdot \mathbf{u} = 0$) reads in dimensionless form

$$\frac{\partial \mathbf{u}}{\partial t} + (\mathbf{u}\,\nabla)\mathbf{u} = -\nabla p + \frac{1}{Re}\Delta \mathbf{u} + N\, g(y^*)\, e^{-\pi \frac{c}{a} y^*}\, \mathbf{e}_t{}^*. \tag{3}$$

Hereby, y^* measures the local wall-normal distance, and $\mathbf{e}_t{}^*$ denotes the corresponding tangential direction vector along the foil. The shape function $g(y^*)$ is zero everywhere except above the active actuator range Δx at the suction side where $g(y^*) = 1$ holds; end effects are approximately taken into account by a linear growth or decay of the force amplitude function $g(y^*)$ in a small transition range at the actuator ends while maintaining the total momentum input. In case of time-periodic forcing, by introducing a nondimensional frequency f based on chord length c and freestream velocity U_0, the shape function above the actuator reads

$$g(y^*, t) = \cos(2\pi\, f\, t), \qquad f = \frac{\tilde{f} \cdot c}{U_0} \tag{4}$$

The two dimensionless characteristic parameter of the problem are

$$Re = \frac{U_0\, c}{\nu}, \qquad N = \frac{\pi}{4}\frac{j_0 B_0 c}{\rho U_0^2} \tag{5}$$

whereby besides the usual Reynolds number Re the interaction parameter N describes the ratio of electromagnetic to inertial forces. Here, ν denotes the kinematic viscosity of the fluid, and $M_0 = 2\, B_0$ is used assuming infinitely long magnets. In analogy to conventional control by blowing, a momentum coefficient may be introduced which describes the ratio of the total momentum added by the Lorentz force to the dynamic pressure. In case of steady control (where $\Delta x \approx 1$ holds) and oscillatory control (based on the rms value of N) the momentum coefficient reads

$$C_\mu = \frac{a\, j_0\, B_0}{2\rho U_0^2} \cdot \frac{\Delta x}{c} = \frac{2\, a}{\pi\, c} N, \qquad c'_\mu = \frac{\sqrt{2}}{2} N^{peak} \frac{2a}{\pi c}\frac{\Delta x}{c}. \tag{6}$$

Forces acting on the hydrofoil are due to friction and pressure but additionally due to action of the Lorentz force. Based on dynamic pressure and chord length, the dimensionless total drag and lift coefficients are defined as $C_D = \frac{F_x}{\frac{\varrho}{2} U_0^2 c}$, $C_L = \frac{F_y}{\frac{\varrho}{2} U_0^2 c}$ where F_x and F_y denote the total force component per spanwise length unit in streamwise and normal direction, respectively. The non-dimensional force input due to the Lorentz force follows from integration over the area above the active part of the actuator and reads for the lift coefficient as (for more details see [17])

$$C_M = \frac{2\, N}{c^2}\left[\int\!\!\int dA\, e^{-\pi \frac{c}{a} y^*}\, \mathbf{e}_t{}^*\right] \cdot \mathbf{e}_y \tag{7}$$

3. DNS

3.1. Simulation Details

A well-established spectral element code was used for the DNS simulations [27, 28] which has already been successfully applied to other EMHD problems [10, 11, 13]. More simulation details can be found in [17]. The computational domain with respect to width and position of the hydrofoil was chosen to resemble the test section geometry of an existing experimental facility and should allow later for comparison with experimental results. Grid generation for hydrofoils at different angles of attack in the rectangular domain was done by using the pre-processing capabilities of FIDAP [29]; typical grids consist of about 200 spectral elements and ensure sufficient resolution at boundary and shear-layer regions in the near wake while trying to avoid computational overhead in low-shear regions. The rectangular domain ranges from $-1 \leq x \leq 7$ and $-1.5 \leq y \leq 1.5$; the center of gravity of the hydrofoil is located at $(x = 0.3,\ y = 0)$. The boundary conditions applied in the simulations are no-slip $(u = 0,\ v = 0)$ at the hydrofoil, freestream $(u = 1,\ v = 0)$ at inlet, top and bottom of the computational domain and an outflow condition at the outlet. At validation runs, for Reynolds numbers up to $Re = 600$ under investigation here, the final choice of 9x9 inner element resolution ensured lift and drag accuracy of about $\pm 1\%$.

3.2. Stationary Forces

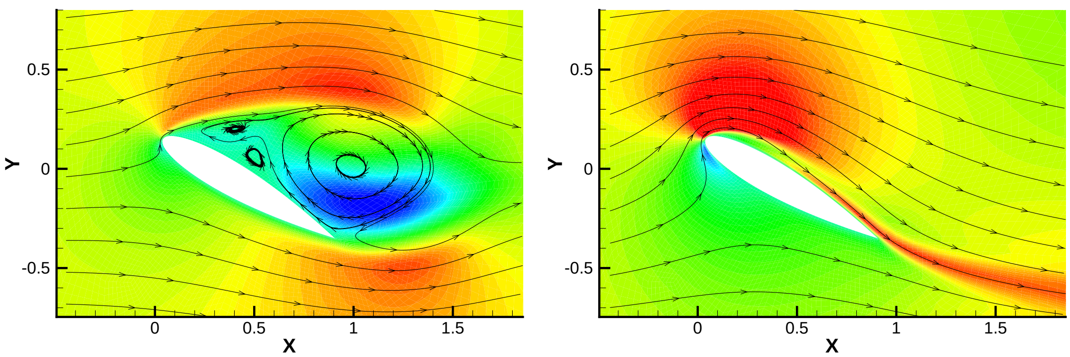

Figure 3. Snapshots of the flow at α=30^o, Re=500 without control (left) and at $C_\mu = 1.61$, $a/c = 0.1265$ (right). Shown are streamtraces und contours of u_x.

Figure 3 shows snapshots of the uncontrolled flow around the hydrofoil at an angle of attack of 30^o and the controlled flow under action of a momentum coefficient of $C_\mu = 1.61$ and a penetration depth of $a/c = 0.1265$ at a Reynolds number of $Re = 500$. The flow without control clearly experiences separation, which can be completely suppressed when applying control. Furthermore, at this large value of the momentum coefficient, the controlled flow is almost steady, and a jet on the suction side can already be detected.

The left side of Figure 4 shows the behavior of the time-averaged lift coefficient as a function of the momentum coefficient at $Re = 600$, $\alpha = 30^o$. Hereby, in the force balance, the momentum input due to the Lorentz force C_M grows only linearly with C_μ whereas the total lift coefficient C_L seems to grow stronger than linearly. For small values of C_μ, a quadratic dependence due to the separation delay is expected, until the flow is completely attached. However, in our numerical investigation, this might be disturbed by the finite channel width which influences the pressure field. The variation of the penetration depth a/c offers a possiblity for reducing the energy

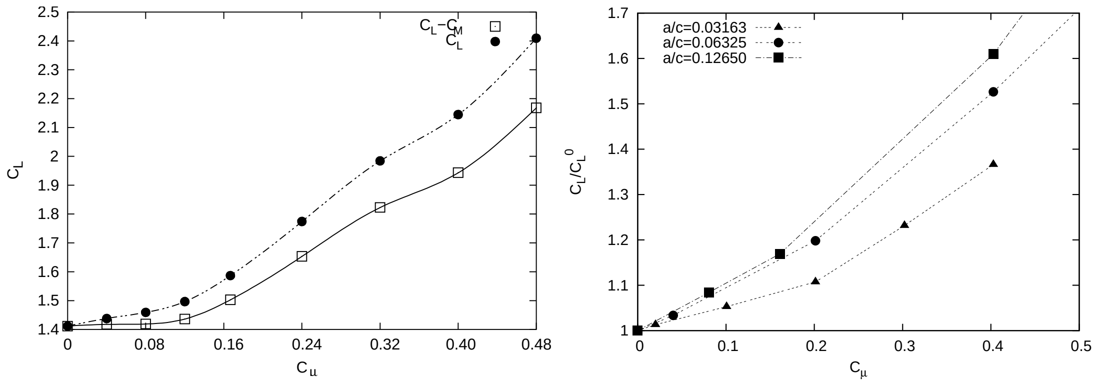

Figure 4. Left: Lift coefficient C_L as a function of the momentum coefficient C_μ. $C_L - C_M$ denotes the part of C_L when the momentum input due to the Lorentz force C_M is not taken into account. Re = 600, $\alpha = 30^o$, $a/c = 0.06325$. Right: Lift gain by variation of the penetration depth a/c at $Re = 500$, $\alpha = 30^o$.

effort needed to achieve some fixed lift gain. The right side of Figure 4 shows the ratio of the lift $C_L(C_\mu)$ at momentum coefficient C_μ divided by the uncontrolled lift C_L^0 versus momentum coefficient C_μ for different values of the penetration depth a/c. For large values of the momentum coefficient, the largest chosen penetration depth performs best. At low control amplitudes, the smallest value of the penetration depth $a/c = 0.03163$ gives only weak lift enhancement. In general, although the lift-optimum penetration depth depends on the details of the flow configuration, it seems to be advantageous to choose a/c not smaller than a characteristic boundary layer thickness of the flow which is $\delta_{lam} \sim 1/\sqrt{Re} \approx 0.044$ in the considered case.

3.3. Oscillatory Forcing

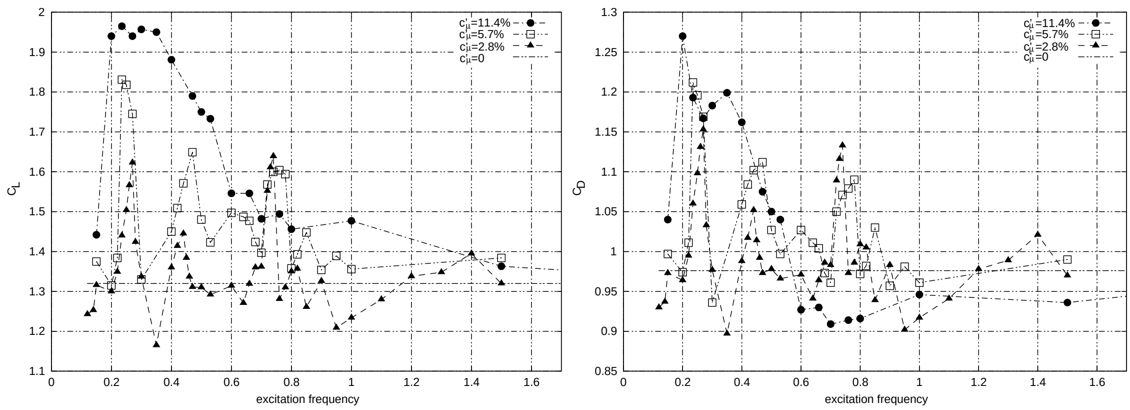

Figure 5. Mean lift coefficient (left) and mean drag coefficient (right) versus excitation frequency at different control amplitudes c'_μ; $a/c = 0.1265$.

Oscillatory actuation was applied at the front part of the hydrofoil, whereby the optimum position of the actuator depends on flow details as, e.g., the position of the separation point. The following results were obtained at a Reynolds number of

$Re = 500$ and an angle of attack of $\alpha = 30^o$ where the uncontrolled flow is already separated (see Fig. 3). Until noted otherwise, an active actuator range of $0.05 \leq x/c \leq 0.15$ was chosen, and the penetration depth of the Lorentz force is $a/c = 0.1265$. Figure 5 summarizes the behaviour of the mean lift and drag coefficient versus actuation frequency f at different values of the momentum coefficient c'_μ. For the weakest control of $c'_\mu = 2.8\%$ applied, there exist distinct maxima for both lift and drag coefficient where a weak control influence is sufficient to advantageously modify the process of vortex shedding. Stronger control in general leads to larger gains in lift but also to larger drag penalties. Interestingly, the control frequencies of the lift maxima are close to the shedding frequency of the uncontrolled flow $f_0 = 0.233$ and its harmonics. With growing control amplitude, largest lift and, at the same time, largest drag, is observed more and more in a broad band of frequencies around the natural shedding frequency, and the importance of higher excitation frequencies decays. The lift gain obtained in the broad frequency band mentioned above corresponds to only a modification of the natural vortex shedding by a strong external excitation. Lock-in behavior of the lift coefficient with the

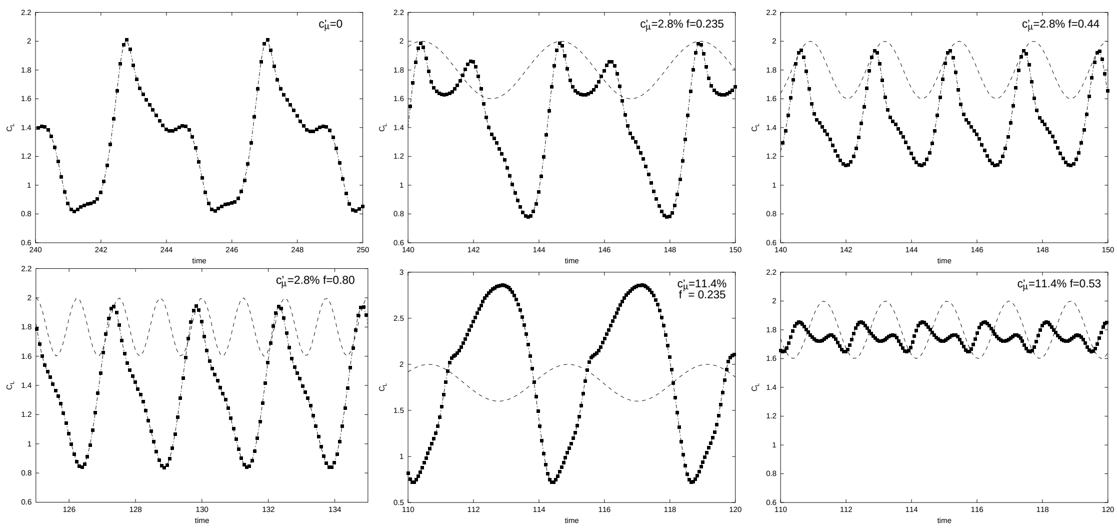

Figure 6. Time signal of the lift coefficient C_L without control and at various values of the interaction parameter N and the control frequency f, superimposed with the corresponding excitation signal of fixed artificial amplitude. Please note a modified C_L-scaling at $c'_\mu = 11.4\%$, $f = 0.235$.

external excitation, well-known from oscillatory cylinder control [22,23,26,30] occurs in certain frequency ranges near the natural shedding frequency f_0 and its harmonics as shown in Fig. 6 for two values of the momentum coefficient. Figure 7 shows streamtraces of the time-averaged flow in case without control and with control at $c'_\mu = 0.11$ for two selected frequencies. As might be also deduced from the size of the separation bubble, control at $f = 0.235$ gives strongly enhanced lift, although the flow does not attach completely, whereas at $f = 0.53$ lift enhancement is already smaller. Although lift enhancement is usually coupled to drag penalty, as can be seen from the left side in Fig. 8, the lift to drag ratio can clearly be enhanced by oscillatory control.

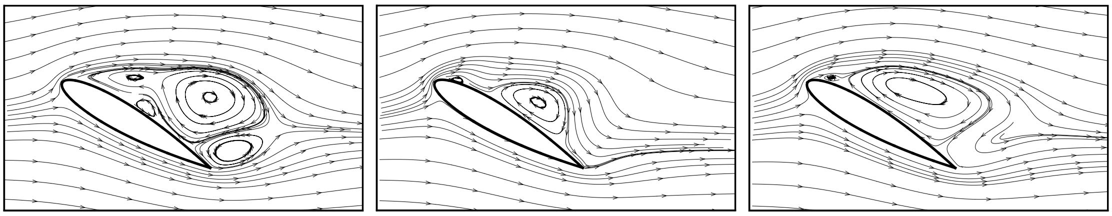

$c'_\mu = 0$ $\qquad$ $c'_\mu = 0.11,\ F^+ = 0.235$ $\qquad$ $c'_\mu = 0.11,\ F^+ = 0.53$

Figure 7. Streamtraces of the time-averaged flow without control (left) and for different control frequencies F^+ at $Re = 500$, $\alpha = 30^o$, $c'_\mu = 0.11$.

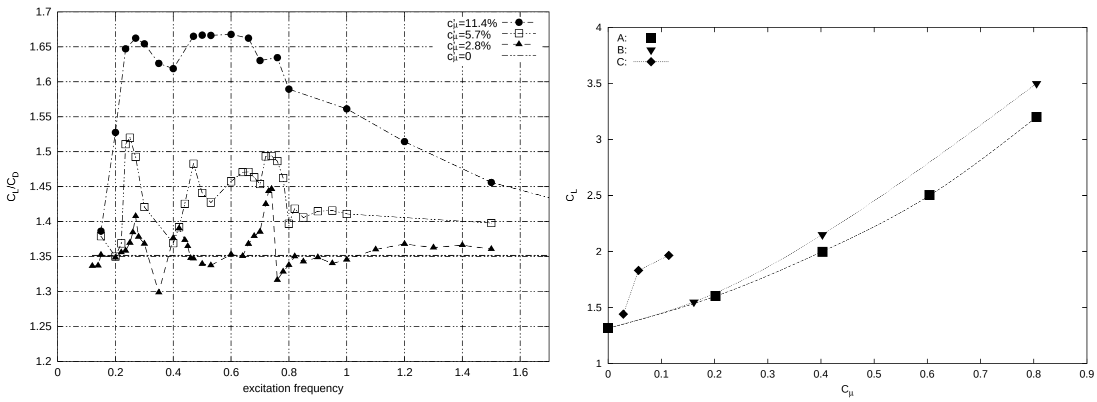

Figure 8. Left: Lift to drag ratio C_L/C_D versus excitation frequency at different amplitudes c'_μ; $a/c = 0.1265$, $\alpha = 30^o$. Right: Comparison of the lift coefficient versus momentum coefficient, obtained by steady (A: $a/c = 0.06325$, B: $a/c = 0.1265$) and oscillatory forcing (C: $a/c = 0.1265$, $f = 0.235$), at $Re = 500$, $\alpha = 30^o$.

3.4. Comparison with steady control

Figure 8 compares on the right side the lift enhancement obtained at the optimum frequency of $f = 0.235$ with results obtained by steady control at different values of the penetration depth a/c. As mentioned above, the larger value of the penetration depth a/c is preferable in case of steady control. But, at small values of the momentum coefficient, oscillatory control is clearly more effective than steady control which here achieves only a small amount of separation delay, whereas oscillatory control is already able to reorganize vortex shedding due to a large receptivity of the uncontrolled flow to optimum control. For larger values of the momentum coefficient, steady forcing might perform better as oscillatory forcing can not completely suppress separation.

4. Turbulent simulations

4.1. Simulation details

First turbulent simulations were performed by using the commercial finite element code FIDAP [29] and applying the extended $k-\epsilon$ model by Chen & Kim [32]. Details of the geometry of the rectangular testsection where also a part of the experimental work was performed can be found in [16], a typical grid consists of about 10000 linear elements with the near-wall resolution is $\Delta^+ \approx 1$ for U-RANS simulations. Top and bottom of the domain are no-slip walls; at inflow, freestream of 2% turbulence level was used to force early transition. Although validation runs for a NACA-0015 profile gave about 10-15% underestimation of the maximum lift at critical angle $C_L^{max}(\alpha_c)$ in general due to obvious lacks in turbulence modelling, as will be seen later, there is a good quantitative agreement of the scaling behavior of ΔC_L^{max} with experimental results.

4.2. Steady control

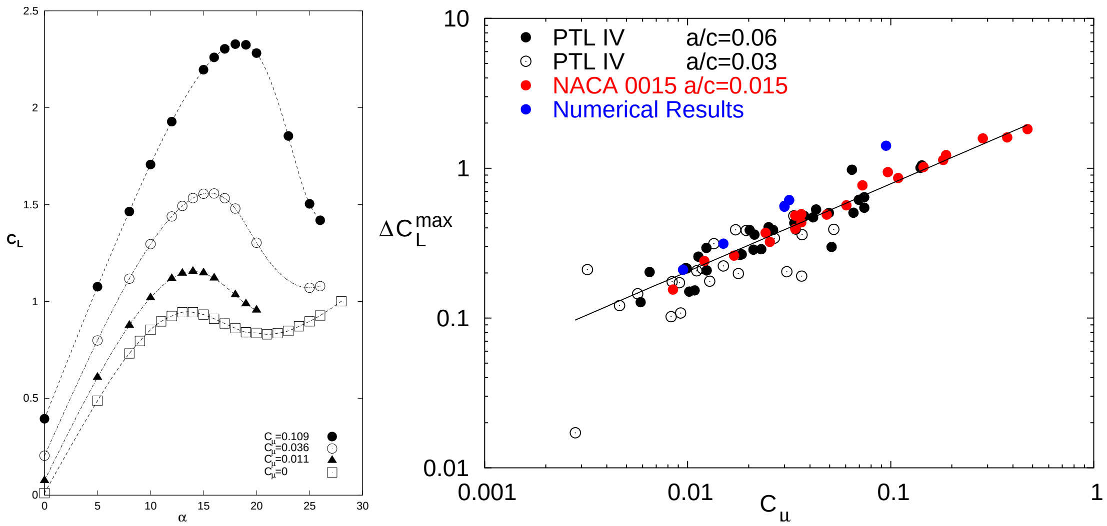

Figure 9. Left: Lift enhancement and delay of stall by steady control at $Re = 800000$, $a/c = 0.06325$; Right: Maximum lift gain versus momentum coefficient by steady control in comparison with experimental results from [15].

Figure 9 shows on the left side the lift enhancement and the delay of stall due to steady control at $Re = 800000$ for different values of the momentum coefficient C_μ. The separation control leads to considerably larger maximum values of the lift coefficient C_L^{max} at larger angles of attack before stall occurs. As for certain applications the maximum lift gain $\Delta C_L^{max} = C_L^{max}(C_\mu) - C_L^{max}(C_\mu = 0)$ as function of C_μ is of importance, on the right side of Fig. 9 the scaling behavior of ΔC_L^{max} versus C_μ is shown in comparison to experimental results of Weier [15]. Apart from the nice agreement, the slight over–estimation of the maximum lift gain obtained numerically as compared to experimental data can be attributed to possible 3-D effects, electrolytic bubble production in the experiment and the simple turbulence model applied. However, the strong effect of separation control can not be found in the figure, as the overall scaling of ΔC_L^{max} is only like $\sim C_\mu^{\frac{1}{2}}$. As the electrical power density can be estimated as $p_E \sim \frac{j_0^2}{\sigma} \sim U_\infty^4 \cdot C_\mu^2$ for steady forcing, the effort for ΔC_L^{max} finally scales as $p_E \sim U_\infty^4 \cdot (\Delta C_L^{max})^4$ which makes applications at large Reynolds numbers energetically expensive. However, larger magnetic fields applied would strongly reduce the energy consumption as $p_E \sim B_0^{-2}$ which gives some future perspective.

4.3. Oscillatory control

First results for oscillatory control are shown at the left side of Fig. 10 for an angle of attack $\alpha = 17^o$ and an active actuator range of $0.07 \leq x/c \leq 0.12$ at $Re = 800000$. As expected, lift-optimum control corresponds to a frequency of $f^+ \approx 1$. Interestingly, lock-in phenomena as described by Wu [3] were also found. The r.h.s. of

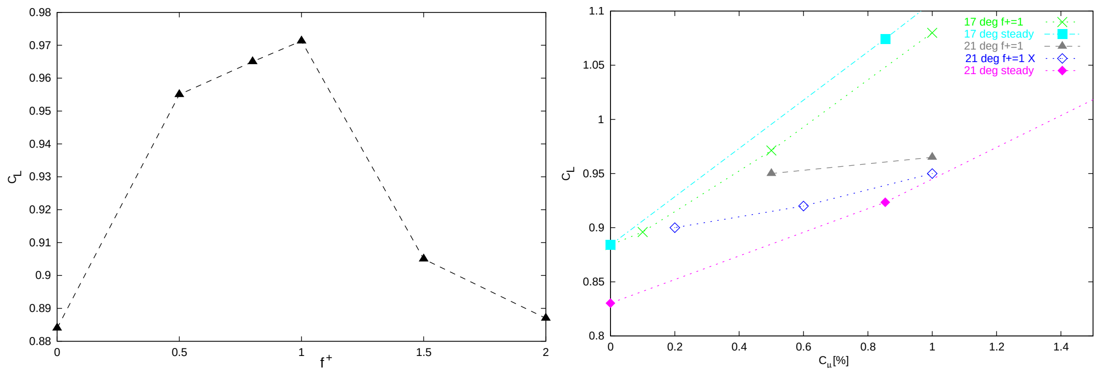

Figure 10. Left: Lift coefficient C_L versus control frequency F^+ at $Re = 800000$, $a/c = 0.06325$, $\alpha = 17^o$. The optimum control frequency is close to one. Right: Comparison of steady and oscillatory forcing at $F^+ = 1$ for $\alpha = 17^o$ and for $\alpha = 21^o$ for which additionally ($\Diamond$) an alternative actuator position $0.02 \leq x/c \leq 0.07$ is shown.

Fig. 10 shows first results of the comparison of steady and periodic control where additionally the case $\alpha = 21^o$ with two different actuator locations was investigated for oscillatory control. As can be seen, in case of $\alpha = 21^o$, for small values of the momentum coefficient C_μ, oscillatory control can be more efficient than steady control, but larger lift gains seem to require similar energy efforts as steady control.

5. Discussion

Control by steady forcing can achieve full reattachement at strong enough control amplitudes but at high cost. Oscillatory control, properly designed with respect to location, frequency and amplitude, can be more efficient for small values of lift enhancement than steady control which can be achieved at small values of the momentum coefficient. Interesting lock-in phenomena were found in both the laminar and the turbulent flow regime which deserve further investigation. Lift-optimum control frequencies as recently noted also in the literature [3,31] were found near the natural shedding frequency of the uncontrolled flow which holds in the laminar and in the turbulent flow regime as oscillatory control always has to struggle with vortex shedding. Currently, more turbulent simulations, also with different modelling, are underway, combined with new PIV measurements of the flow.

Acknowledgements

We are grateful to G.E. Karniadakis and his group at Brown University for introducing us into the code PRISM. The computations were performed at the computing center of Forschungszentrum Dresden-Rossendorf. Financial support from DFG in frame of Sonderforschungsbereich 609 is gratefully acknowledged.

References

[1] M. Gad-el-Hak, *Flow Control*, Cambridge University Press, 2000.

[2] D. Greenblatt, I.J. Wygnanski, *The control of flow separation by periodic excitation*, Prog. Aero. Sci. **36** (2000) 487-545.

[3] J.-Z. Wu, X.-Y. Lu, A.G. Denny, M. Fan and J.-M. Wu, *Post-stall flow control on an airfoil by local unsteady forcing*, J. Fluid Mech. **371** (1998) 21-58.

[4] E.L. Resler & W.R.Sears, *The prospects for magneto-aerodynamics*, J.Aero.Sci. **25** (1958) 235-245.

[5] A. Gailitis, O. Lielausis, *On the possibility to reduce the hydrodynamical resistance of a plate in an electrolyte*, Appl. Magnetohydrodyn. Rep. Riga Inst. Phys. 12 (1961) 143-146 (in Russian).

[6] T.Albrecht, R.Grundmann, G.Mutschke, G.Gerbeth: On the stability of the boundary layer subject to a wall-parallel Lorentz force. Phys. Fluids **18** (2006) 098103.

[7] C. Henoch and J. Stace, *Experimental investigation of a salt water turbulent boundary layer modified by an applied streamwise magnetohydrodynamic body force*, Phys. Fluids **7** (1995) 1371–1383.

[8] C. Crawford and G. E. Karniadakis, *Reynolds stress analysis of EMHD-controlled wall turbulence. Part I. Streamwise forcing* Phys. Fluids **9** (1997) 788–806.

[9] T.W. Berger, J. Kim, C. Lee and L. Lim, *Turbulent boundary layer control utilizing the Lorentz force*, Phys. Fluids **12** no. 3 (2000) 631–649.

[10] Y. Du and G.E. Karniadakis, *Suppressing Wall Turbulence by Means of a Transverse Travelling Wave*, Science **288** (2000) 1230-1234.

[11] Yiqing Du, V. Symeonidis and G. E. Karniadakis, *Drag reduction in wall-bounded turbulence via a transverse travelling wave*, J.Fluid Mech. **457** (2002) 1-34.

[12] V.Shatrov, G.Gerbeth: *Magnetohydrodynamic drag reduction and its efficiency*, Phys. Fluids **19** (2007) 035109

[13] O. Posdziech and R. Grundmann, *Electromagnetic control of seawater flow around circular cylinders*, Eur. J. Mech.-B/Fluids **20** (2001) 255-274.

[14] S.-J. Kim and C.M. Lee, *Investifation of the flow around a circular cylinder under the influence of an electromagnetic force*, Exp. Fluids **28** (2000) 252-260.

[15] T. Weier, G. Gerbeth, G. Mutschke, O. Lielausis and G. Lammers, *Control of Flow Separation Using Electromagnetic Forces*, Flow, Turbulence and Combustion **71** (2003) 5–17.

[16] T. Weier and G. Gerbeth, *Control of Separated Flows by Time-Periodic Lorentz Forces*, Eur. J. Mech./B - Fluids **23** (2004) 835–849.

[17] G.Mutschke, G.Gerbeth, T.Albrecht, R.Grundmann: *Separation Control at Hydrofoils using Lorentz Forces*, Eur. J. Mech./B - Fluids **25** (2006) 137–152.

[18] D. Greenblatt, I. Wygnanski, *Use of periodic excitation to enhance airfoil performance at low Reynolds numbers*, J. Aircraft **38** (2001) 190–192.

[19] Y.Hoarau, M.Braza, Y.Ventikos, D.Faghani, G.Tzabiras: *Organized modes and the three-dimensional transition to turbulence in the incompressible flow around a NACA0012 wing*, J. Fluid Mech. **496** (2003) 63–72.

[20] T. Weier, G. Gerbeth, G. Mutschke, E. Platacis and O. Lielausis, *Experiments on cylinder wake stabilization of an electrolyte solution by means of electromagnetic forces localized on the cylinder surface*, Exp. Therm. Fluid Science **16** (1998) 84-91.

[21] P. Poncet, *Vanishing of mode B in the wake behind a rotationally oscillating circular cylinder*, Phys. Fluids **14** no. 6 (2002) 2021-2023.

[22] G.E. Karniadakis and G.S. Triantafyllou, *Frequency selection and asymptotic states in laminar wakes*, J. Fluid Mech. **199** (1989) 441–469.

[23] S. Choi, H. Choi and S. Kang, *Characteristics of flow over a rotationally oscillating cylinder at low Reynolds number*, Phys. Fluids **14** no. 8 (2002) 2767-2777.

[24] T. Weier, G. Gerbeth, G. Mutschke, U. Fey, O. Posdziech, O. Lielausis and E. Platacis, *Some results on electromagnetic control of flow around bodies*, Proc. Int. Symp. "Seawater Drag Reduction", Newport, R.I., July 22-24, 1998.

[25] S. Taneda, *Visual Observations of the Flow past a Circular Cylinder Performing a Rotary Oscillation*, J. Phys. Soc. Jpn. **45** (1978) 3114-3116.

[26] P.T. Tokumaru and P.E. Dimotakis, *Rotary oscillation control of a cylinder wake*, J. Fluid Mech. **224** (1991) 77-90.

[27] R.D. Henderson and G.E. Karniadakis, *Unstructured spectral element methods for simulation of turbulent flows*, J. Comp. Phys. **122** (1995) 191–217.

[28] G.E. Karniadakis and S.J. Sherwin, *Spectral/hp Element methods for CFD*, Oxford University Press, 1999.

[29] FIDAP 8.0; Fluent Inc., 2002.

[30] S. Mittal, *Control of flow past bluff bodies using rotating control cylinders*, J. Fluids Struct. **15** (2001) 291-326.

[31] A. Darabi and I. Wygnanski, *Active management of naturally separated flow over a solid surface. Part 1. The forced reattachement process*, J. Fluid Mech. **510** (2004) 105–129.

[32] Y.S.Chen, S.W.Kim, *Computation of Turbulent Flows Using an Extended k-ϵ Turbulence Closure Model*, NASA CR 179204, 1987.